The Cryosphere
Open Access
Discussions

A prognostic model of the sea ice floe size and thickness distribution

C. Horvat and E. Tziperman

School of Engineering and Applied Sciences and Department of Earth and Planetary Sciences, Harvard University, Cambridge, MA, USA

Correspondence to: C. Horvat (horvat@fas.harvard.edu)

Discussion Paper | Discussion Paper | Discussion Paper | Discussion Paper

Title Page

Abstract	Introduction
Conclusions	References
Tables	Figures

| ◄ | ► |
| ◄ | ► |

Back | Close

Full Screen / Esc

Printer-friendly Version

Interactive Discussion

Abstract

Sea ice exhibits considerable seasonal and longer-term variations in extent, concentration, thickness and age, and is characterized by a complex and continuously changing distribution of floe sizes and thicknesses. Models of sea ice used in current climate models keep track of its concentration and of the distribution of ice thicknesses, but do not account for the floe size distribution and its potential effects on air–sea exchange and sea-ice evolution. Accurately capturing sea-ice variability in climate models may require a better understanding and representation of the distribution of floe sizes and thicknesses. We develop and demonstrate a model for the evolution of the joint sea-ice floe size and thickness distribution that depends on atmospheric and oceanic forcing fields. The model accounts for effects due to multiple processes that are active in the marginal and seasonal ice zones: freezing and melting along the lateral side and base of floes, mechanical interactions due to floe collisions (ridging and rafting) and sea-ice fracture due to swell propagation into the ice pack. The model is then examined and demonstrated in a series of idealized test cases.

1 Introduction

Sea ice is a major component of the climate system, covering about 12 % of the ocean surface. It drives the ice-albedo feedback, a potential source of climate instability and polar amplification, and it affects deep water formation and air–sea fluxes of heat, fresh water and momentum between the atmosphere and ocean. Its presence also provides a platform for high-latitude ecosystems and determines polar shipping routes. Additionally, sea ice is well-correlated with patterns of atmospheric variability such as the North Atlantic Oscillation (Strong et al., 2009), the Antarctic Oscillation (Wu and Zhang, 2011), and the Madden-Julian Oscillation (Henderson et al., 2014). Over the past few decades, Arctic sea ice has become thinner, less extensive, and more seasonal (Cavalieri and Parkinson, 2012). Regions that were once covered by ice year-round now

are ice-free in the summer (Stroeve et al., 2012), and the Arctic marginal ice zone, defined as the area of ice with concentration between 15 and 80 %, has been widening during the summer season (Strong and Rigor, 2013). High-latitude storms are capable of breaking thinning pack ice into smaller floes, changing ocean circulation and air–sea exchange (Asplin et al., 2012; Zhang et al., 2013), with evidence suggesting that these storms will become more prevalent in the future (Vavrus et al., 2012).

Sea-ice cover is heterogeneous, composed of a distribution of floes of different areas and thicknesses. Floes can vary dramatically in size, ranging from newly-formed frazil crystals millimeters in size to pack ice in the Canadian Arctic with floes up to ten meters thick in places and hundreds of kilometers wide. As sea-ice cover becomes thinner and more fractured, the distribution of these floes and their size, shape, and properties may change. Events that generate surface waves, such as a fortuitously observed Arctic cyclone in 2011, the so-called "Great Arctic Cyclone" of 2012, and an energetic wave event observed in the Barents sea, can lead to the fracturing of floes (Asplin et al., 2012; Zhang et al., 2013; Collins et al., 2015). The fractured sea-ice cover has increased floe perimeter, which may lead to enhanced melting and a more rapid reduction in sea-ice area compared to an unfractured sea-ice cover (Steele, 1992), and may lead to changes in the mechanical response of the sea-ice cover to forcing from the ocean and atmosphere (Feltham, 2005). As sea ice attenuates wave energy, the diminished ice fraction may lead to further surface wave propagation into the ice field, enhancing fracturing farther from the sea-ice edge, and leading to further sea-ice area loss in a positive feedback loop (Asplin et al., 2014). Along floe edges, ocean eddies may be generated due to the gradient in surface heat and stress boundary conditions between ice edge and open water (Niebauer, 1982; Johannessen et al., 1987). These eddies may more rapidly mix air–sea heat flux absorbed by open water to underneath sea-ice floes when floe sizes are comparable to the eddy length scale, but not when floe sizes are much larger. This in turn may have consequences for ice melt rates and ocean circulation (Horvat and Tziperman, 2015).

Given that it is not computationally practical to simulate all individual floes, properties of the ice cover can instead be described using statistical distributions. This approach was pioneered by Thorndike et al. (1975), who developed a framework for simulating the thickness distribution (ITD), $g(h)$, defined such that $g(h)\mathrm{d}h$ is the fractional area of the sea surface covered by ice with thickness between h and $h + \mathrm{d}h$. The Thorndike model evolves the prognostic equation

$$\frac{\partial g(h)}{\partial t} = -\nabla \cdot (g\boldsymbol{u}) - \frac{\partial}{\partial h}(g(h)\dot{h}) + \psi, \tag{1}$$

where $\boldsymbol{u}$ is the horizontal ice velocity, $\dot{h}$ is the rate of change of ice thickness due to melting and freezing (thermodynamics), and ψ, the "redistribution function", describes the creation of ice of thickness h by mechanical combination of ice of different thicknesses. Measurements of ice thickness are made possible by a variety of remote sensing techniques such as submarine sonar, fixed moorings, helicopter borne electromagnetic induction, and satellite measurements (Bourke and Garrett, 1987; Yu and Rothrock, 1996; Renner and Gerland, 2014), which may be used to test model skill. Variants of the Thorndike model have been implemented in several general circulation models (GCMs, Bitz, 2008; Hunke et al., 2013), and have been used to understand sea ice behavior and predictability (Bitz et al., 2001; Chevallier and Salas-Mélia, 2012).

Modern approaches to modeling sea ice in GCMs, such as the community ice model (Hunke et al., 2013), generally approximate ice cover as a non-Newtonian fluid with a vertically layered thermodynamics, and simple thickness distribution (Thorndike et al., 1975; Semtner, 1976; Hibler, 1979). This level of detail may not suffice in regions where ice cover is heterogeneous and variable (Birnbaum and Lüpkes, 2002; Girard et al., 2009), as it does not account for the lateral size distribution of floes.

We aim to describe the sub-grid scale variability of the sea-ice cover by extending the ice thickness distribution to a joint distribution that includes both ice thickness and floe size. Rothrock and Thorndike (1984) were among the first to describe the distribution of lateral floe sizes, defining the floe size distribution (FSD) $n(r)\,\mathrm{d}r$ as the fractional area

of the sea surface covered by floes with lateral size between r and $r + dr$. The size of a floe with area a is represented by its effective radius, $r = \sqrt{a/\pi}$, which represents floes as cylinders of radius r. Modeling of the lateral floe size distribution is hampered by the difficulty of measurement, as floe sizes vary over many orders of magnitude.

Such physical systems require a large observational window in order to avoid truncation errors that under-sample large elements (Lu et al., 2008). Even with sufficient imagery, algorithms that identify and measure floes must overcome many obstacles, such as submerged floes, melt ponds, and clouds. In spite of these challenges, many point observations of the floe size distribution have been successfully made, often using helicopter or ship-board cameras (Holt and Martin, 2001; Toyota and Enomoto, 2002; Toyota et al., 2006, 2011; Lu et al., 2008; Herman, 2010). These studies have focused on deriving and fitting scaling relationships measured distributions, leading to power-law (Toyota et al., 2006), Pareto (Herman, 2010), or joined power-law (Toyota et al., 2011) distributions of floe sizes. The temporal evolution of the floe size distribution has been examined in a small number of observational studies (Holt and Martin, 2001; Steer et al., 2008; Perovich and Jones, 2014), that analyzed the change in the floe size distribution over several weeks or seasonally, but these observations, particularly in the marginal ice zone, are limited. Analytic studies involving the evolution of the floe size distribution have mainly focused on understanding ocean wave propagation and attenuation in the marginal ice zone (Dumont et al., 2011; Williams et al., 2013).

Zhang et al. (2015) developed a model to simulate floe size distribution evolution, assuming that all floes of different sizes have same ITD. The present paper, however, develops a model for the *joint* floe size and thickness distribution, allowing for different ice thickness distribution for each horizontal size class. The Zhang et al. (2015) paper shares many of our goals and we refer to it below, further elaborating on additional differences between the two studies in the treatment of thermodynamics, mechanical interactions and wave fracturing.

The purpose of the present paper is to develop and demonstrate a framework for modeling the joint distribution of floe sizes and thicknesses (referred to below as the

FSTD) $f(r,h)$, with $f(r,h)\mathrm{d}r\mathrm{d}h$ being the fraction of the ocean surface area covered by floes of thickness between h and $h + \mathrm{d}h$ and lateral size between r and $r + \mathrm{d}r$ (a list of variable names and descriptions are provided in Table 1). The ice thickness distribution $g(h)$ and floe size distribution $n(r)$ are obtained by integrating over the joint distribution $f(r,h)$,

$$g(h) = \int_0^\infty f(r,h)\mathrm{d}r,$$

$$n(r) = \int_0^\infty f(r,h)\mathrm{d}h.$$

The prognostic equation for the joint floe size and thickness distribution has the form,

$$\frac{\partial f(\mathbf{r})}{\partial t} = -\nabla \cdot (f(\mathbf{r})\,\boldsymbol{u}) + \mathcal{L}_\mathrm{T} + \mathcal{L}_\mathrm{M} + \mathcal{L}_\mathrm{W}, \tag{2}$$

where $\mathbf{r} = (r,h)$. The term $\nabla \cdot (f(\mathbf{r})\,\boldsymbol{u})$ describes advection of the floe size distribution by the flow of ice. $\mathcal{L}_\mathrm{T}$ is the time rate of change of the floe size distribution due to thermodynamic effects. $\mathcal{L}_\mathrm{M}$ is the time rate of change due to mechanical interaction (rafting and ridging of floes). $\mathcal{L}_\mathrm{W}$ is the time rate of change due to floes being fractured by surface ocean waves. We parameterize each of the above processes, forced by grid-scale atmospheric and oceanic forcing fields.

The paper proceeds as follows: we first develop explicit representations for the different processes affecting the joint floe size and thickness distribution in response to atmospheric and oceanic forcing (Sect. 2). The model response to individual forcing fields, in the form of air–sea heat fluxes, ice flow that leads to floe collisions, and surface waves, is analyzed in Sect. 3. We conclude in Sect. 4.

2 Representing processes that affect the joint floe size and thickness distribution

2.1 Thermodynamics

Air–sea heat fluxes in the polar oceans lead to the freezing and melting of ice. In regions of open water, cooling produces frazil ice which may consolidate with other floes or form pancakes. When floes grow due to the accumulation of frazil crystals, or by congelation growth at their bases, their size and thickness will change, but the total number of floes will not. Suppose that the only source or sink of ice volume is due to freezing and melting of existing floes, which causes them to change their size and thickness at a rate $G = (\dot{r}, \dot{h})$. Let N be the number distribution, such that $N(\boldsymbol{r})\,dh\,dr$ is the number of floes in the range $(h, h + dh)$, $(r, r + dr)$ (a list of the variables used to describe FSTD thermodynamics is provided in Table 2). The cumulative number distribution is defined as $C(\boldsymbol{r}) = \int_0^r N(\boldsymbol{r}')\,d\boldsymbol{r}' = \int_0^r (f(\boldsymbol{r}')/\pi r'^2)\,d\boldsymbol{r}'$, with $\frac{\partial^2}{\partial r \partial h}(C) = N(\boldsymbol{r}) = f(\boldsymbol{r})/\pi r^2$, and it obeys the conservation equation,

$$C(\boldsymbol{r}, t) = C(\boldsymbol{r} + \boldsymbol{G}\,dt, t + dt),$$

since floes with a finite size and thickness $\boldsymbol{r} = (r, h)$ are, by assumption, neither created nor destroyed by thermodynamic growth and melting. Expanding the right hand side and rearranging in the limit as $dt \to 0$ leads to the time rate of change of the cumulative number distribution,

$$\frac{\partial C(\boldsymbol{r}, t)}{\partial t} = -\boldsymbol{G} \cdot \nabla_{\boldsymbol{r}} C, \tag{3}$$

where $\nabla_{\boldsymbol{r}} = (\frac{\partial}{\partial r}, \frac{\partial}{\partial h})$ is the vector of partial derivatives in (size, thickness) space. Changes to the cumulative number distribution are due to the transfer of ice to larger or smaller sizes by thermodynamic growth and melting. We next make the assumption that thickness changes due to melting and freezing do not depend on the

floe radius, and that horizontal size changes do not depend on the thickness, i.e., $\frac{\partial}{\partial h}\left(\frac{\partial r}{\partial t}\right) = \frac{\partial}{\partial r}\left(\frac{\partial h}{\partial t}\right) = 0$. The time evolution of the floe size distribution solely due to freezing and melting of existing floes is derived by taking derivatives with respect to both thickness and size of Eq. (3),

$$\left.\frac{\partial f(r)}{\partial t}\right|_{\text{melt/freeze}} = -\pi r^2 \frac{\partial}{\partial r}\left(\frac{f(r)}{\pi r^2}\frac{\partial r}{\partial t}\right) - \frac{\partial f(r)}{\partial h}\frac{\partial h}{\partial t},$$

$$= -\nabla_r \cdot (f(r)G) + \frac{2}{r}f(r)\frac{\partial r}{\partial t}. \tag{4}$$

Without loss of generality, consider the interpretation of this equation for the case of freezing in which existing floes get thicker and larger. This implies that some of the area $f(r)$ now moves to larger ice classes, represented by the first term in Eq. (4). Note that the integral over all size classes and thickness of the first term vanishes, and therefore it does not describe ice area growth. The total ice area added or removed that belongs to floes of size r, $N(r)\mathrm{d}/\mathrm{d}t(\pi r^2)$, equal to $N(r)2\pi r\mathrm{d}r/\mathrm{d}t$, which is equal to the second term in Eq. (4).

Zhang et al. (2015) include the effects of melting and freezing on the FSD, in a way that depends on the lateral growth rate (our $\dot{r}$), but without evaluating this rate in terms of thermodynamic forcing. Their formulation seems to lack the second term on the rhs of Eq. (4). The formulation presented here is for the joint FSTD, and therefore depends on both $\dot{r}$ and $\dot{h}$. We further evaluate these rates below in terms of air–sea fluxes.

In addition to melting and freezing of existing floes we must also consider the rate of growth of pancake ice, $\dot{A}_p$, due to the flocculation of frazil crystals in patches of open water away from existing floes. Pancakes are assumed to be created by freezing at the smallest size and thickness accounted for in the model, with an effective radius r_p and thickness h_p. The full expression for the rate of change of the floe size and thickness distribution due to thermodynamics, $\mathcal{L}_T$, is therefore,

$$\mathcal{L}_T = -\nabla_r \cdot (f(r)G) + \frac{2}{r}f(r)\frac{\partial r}{\partial t} + \delta(r_p, h_p)\dot{A}_p. \tag{5}$$

The floe size and thickness change rate vector $G = (\partial r / \partial t, \partial h / \partial t)$ is determined using the balance of heat fluxes at the ocean/ice/atmosphere interface. Note that our focus here is the impact of thermodynamic forcing on the FSTD: we are not modeling internal ice thermodynamics explicitly. In an application of the FSTD model, a full thermodynamic model of the ocean mixed layer and sea ice would simulate the ice energy budget. Net heat flux in ocean regions adjacent to ice floes (which we refer to as lead regions) is assumed to affect the development of adjacent floes laterally and vertically, while cooling in open water away from existing floes may lead to pancake ice formation (the model does not resolve frazil ice, nor arbitrarily small pancake ice). The lead region is defined as the annulus around each floe of width r_p, and the division of ocean area into lead and open water areas is shown as the blue and white regions in Fig. 1, (see also Parkinson and Washington, 1979). The total lead area, A_{lead}, is approximated as,

$$A_{lead} = \min \left(\iint_r \left(N(r) \pi (r + r_p)^2 - N(r) \pi r^2 \right) dr, \phi \right)$$

$$= \min \left(\iint_r f(r) \left(\frac{2 r_p}{r} + \frac{r_p^2}{r^2} \right) dr, \phi \right),$$

where ϕ is the open water fraction, and the above integration is over the entire ranges of effective radius and thickness represented in the model. A net air–sea heat flux Q at the ocean surface is therefore partitioned into a lead heat flux $Q_{lead} = A_{lead} Q$ and an open water heat flux $Q_o = (\phi - A_{lead}) Q$. If the water is at its freezing point, a cooling heat flux leads to freezing of pancakes of ice of radius r_p and thickness h_p, producing the area $\dot{A}_p$ of ice pancakes per unit time where there was formerly open water,

$$\dot{A}_p = \frac{Q_o}{\rho_0 L_f h_p}.$$

Title Page

Abstract | Introduction

Conclusions | References

Tables | Figures

|◄ | ►|

◄ | ►

Back | Close

Full Screen / Esc

Printer-friendly Version

Interactive Discussion

C. Horvat and
E. Tziperman

The lead region heat flux, Q_{lead}, is further partitioned into a part that leads to basal freezing or melting of existing ice floes, $Q_{l,b}$, and a component that leads to lateral freezing or melting along perimeters of existing floes, $Q_{l,l}$. Multiple choices for this partitioning are possible, including a binary partition (Washington et al., 1976) with $Q_{l,b} = Q_{lead}$, $Q_{l,l} = 0$ or $Q_{l,l} = Q_{lead}$, $Q_{l,b} = 0$, a parameterization with a quadratic dependence on open water fraction $Q_{l,l} \propto A_{lead}^2$ (Parkinson and Washington, 1979), and diffusive and molecular-sublayer parameterizations based on the temperature of the surface waters (Steele, 1992; McPhee, 1992). While these parameterizations have been tested in some detail (Harvey, 1990; Steele, 1992), sensitivity analyses in previous studies have fixed (either explicitly or implicitly) the floe size distribution, and the impact of this assumption on the results is unclear. We choose to simply assume that the lead heat flux is mixed uniformly over the exposed surface of a floe, partitioned according to the ratio of ice basal and lateral surface areas, where it contributes to ice growth or melt. The total fractional lateral surface area (that is, the area of the vertical edges of ice floes, per unit ocean area) is

$$\iint_r N(r)2\pi r h\, dr = \iint_r f(r)\frac{2h}{r}\, dr = \overline{2h/r},$$

where N is the number distribution introduced above, $2\pi r h$ is the lateral area of one floe, and $\overline{2h/r}$ represents an average over all ice floes, weighted by the floe size and thickness distribution. The total basal ice surface area per unit ocean area is the ice concentration, c. The partitioning of heat flux from the lead region between the ice base and ice edges is therefore,

$$Q_{l,l} = Q_{lead}\left(1 + \frac{c}{\overline{2h/r}}\right)^{-1}; \quad Q_{l,b} = Q_{lead}\left(1 + \frac{\overline{2h/r}}{c}\right)^{-1}.$$

The rate of change of ice thickness can be found using a model of ice thermodynamics, given the above derived open-water air–sea flux contribution $Q_{l,b}$ to the heat budget at

the ice base. For example, ignoring ice heat capacity, ice thickness changes due to melting and freezing are related to the net heat flux into the ice from the surface above, Q_{surf} (defined negative upward), and from below (where negative flux means ocean cooling),

$$\rho_i L_f \frac{\partial h}{\partial t} = -(Q_{l,b} + Q_{surf}).$$ (6)

The rate of change of the lateral floe size is calculated from the corresponding contribution of the air–sea heat flux from the lead region $Q_{l,l}$,

$$\rho_i L_f \frac{\partial r}{\partial t} = -Q_{l,l}.$$ (7)

The above equations can now be used to express the thermodynamic floe growth rate vector, $\boldsymbol{G} = (\dot{r}, \dot{h})$.

2.2 Mechanical interactions

Wind and ocean currents can drive individual floe collisions, and therefore merge them together. When one floe overrides another while remaining intact, the interaction is referred to as rafting. If the ice at the point of contact disintegrates into a rubble pile, forming a "sail" and a "keel", and the two floes consolidate, the interaction is referred to as ridging. To describe these processes, open water in the floe size and thickness distribution $f(r)$ is represented by a delta function at $r = 0$, multiplied by the area fraction of open water. The dynamics of open water formation by ice flows may then be derived by taking integrals over the prognostic equation (Eq. 2) that include or exclude $r = 0$ (a list of the variables used to describe the FSTD response to floe collisions is provided in Table 3). Since the integral of $f(r)$ over all floe sizes including zero is equal to 1, ignoring thermodynamic and wave effects, and including the contribution of open water by taking the integral of Eq. (2) over a range of floe sizes that includes a vanishingly

small interval of sizes around $\boldsymbol{r} = (r, h) = \boldsymbol{0}$,

$$\int_{\boldsymbol{0}^-} \mathcal{L}_M(\boldsymbol{r})\,\mathrm{d}\boldsymbol{r} \equiv \lim_{|(\epsilon_1,\epsilon_2)|\to 0} \int_{-\epsilon_1}^{\infty}\int_{-\epsilon_2}^{\infty} \mathcal{L}_M(r,h)\,\mathrm{d}r\mathrm{d}h,$$

$$= \int_{\boldsymbol{0}^-} \left[\frac{\partial f(\boldsymbol{r})}{\partial t} + \nabla\cdot(f(\boldsymbol{r})\,\boldsymbol{u})\right]\mathrm{d}\boldsymbol{r},$$

$$= \frac{\partial 1}{\partial t} + \nabla\cdot(1\,\boldsymbol{u}) = \nabla\cdot\boldsymbol{u}. \tag{8}$$

Next, as the integral of $f(\boldsymbol{r})$ over all floe sizes, but excluding open water, is equal to the ice concentration c, integrating Eq. (2) again but excluding $\boldsymbol{r} = 0$,

$$\int_{\boldsymbol{0}^+} \mathcal{L}_M(\boldsymbol{r})\mathrm{d}\boldsymbol{r} \equiv \lim_{|(\epsilon_1,\epsilon_2)|\to 0} \int_{\epsilon_1}^{\infty}\int_{\epsilon_2}^{\infty} \mathcal{L}_M(r,h)\mathrm{d}r\mathrm{d}h,$$

$$= \int_{\boldsymbol{0}^+} \left[\frac{\partial f(\boldsymbol{r})}{\partial t} + \nabla\cdot(f(\boldsymbol{r})\,\boldsymbol{u})\right]\mathrm{d}\boldsymbol{r},$$

$$= \frac{\partial c}{\partial t} + \boldsymbol{u}\cdot\nabla c + c(\nabla\cdot\boldsymbol{u}) \equiv \frac{D_M c}{Dt}. \tag{9}$$

The above definition of operator D_M/Dt implies that $D_M(1)/Dt = \nabla\cdot\boldsymbol{u}$. The subscript M indicates that this operator represents concentration changes due to mechanical interactions only. $D_M c/Dt$ is equal to the total sea-ice area which is eliminated due to the collisions of floes per unit time. Subtracting Eq. (8) from Eq. (9),

$$\int_{\boldsymbol{0}^-}^{\boldsymbol{0}^+} \mathcal{L}_M(\boldsymbol{r})\mathrm{d}\boldsymbol{r} = \nabla\cdot\boldsymbol{u} - \frac{D_M c}{Dt}.$$

This result implies that $\mathcal{L}_M(r)$ has a $\delta(r)$ component due to open water creation in floe collisions, or the integral on the infinitesimally small range near zero size would have vanished. In addition, Eq. (9) suggests that there should be another term in $\mathcal{L}_M(r)$ that, when integrated over all sizes leads to $D_M c/Dt$. This suggests the following form,

$$\mathcal{L}_M = (\nabla \cdot \boldsymbol{u})\delta(r) + \frac{D_M c}{Dt}\left[L_c(r) - \delta(r)\right], \tag{10}$$

where $L_c(r)$ is yet unspecified except that its integral over all sizes is one, and it is non-singular at $\|r\| = 0$,

$$\int_{0^+} L_c(r)\, dr = \int_{0^-} L_c(r)\, dr = 1. \tag{11}$$

The factor $L_c(r)$ quantifies the relative fraction of the total concentration lost due to collisions at each floe size. The terms in Eq. (10) that are proportional to $\delta(r)$ represent together the formation of open water due to collisions driven by divergent ice motions. The remaining term represents the rearrangement of ice area among floe classes. It remains to derive expressions for the rate of open water formation due to collisions $D_M c/Dt$, and the rearrangement of the floe size and thickness distribution in response to a unit amount of open water formation due to collisions, $L_c(r)$.

Thorndike et al. (1975) described the rate of mechanical interactions as depending on the divergence, convergence and shear of the ice flow, weighted by the relative size of the invariants of the ice strain rate tensor $\dot{\boldsymbol{e}}$,

$$\dot{e}_{ij} = \frac{1}{2}\left(\frac{\partial u_i}{\partial x_j} + \frac{\partial u_j}{\partial x_i}\right). \tag{12}$$

Defining the deviatoric strain tensor, $\dot{e}'_{ij} = \dot{e}_{ij} - \delta_{ij}\nabla \cdot \boldsymbol{u}/2$, equal to the divergence-free part of $\dot{e}_{ij}$, two relevant invariants may be written as $\boldsymbol{E} = (e_I, e_{II}) = (\nabla \cdot \boldsymbol{u}, 2|-\dot{e}'|^{1/2})$. The

first invariant is the flow divergence and the second is calculated from the determinant of the deviatoric strain rate tensor, and is equal to the maximal shear strain rate. Given these definitions, we parameterize the rate of ice area loss due to collisions as,

$$\frac{D_M c}{Dt} = \frac{1}{2}\left(\epsilon_I - \|E\|\right) \leq 0,$$ (13)

which allows us to write the mechanical interaction term in the FSTD equation as,

$$\mathcal{L}_M = \delta(r)\epsilon_I + \frac{1}{2}\left(\|E\| - \epsilon_I\right)\left[\delta(r) - L_c\right].$$ (14)

This formulation is exactly equivalent to that of Thorndike et al. (1975), see Appendix for details. In the case of ice flow characterized by pure divergence, $E = (\nabla \cdot u, 0)$ and $\nabla \cdot u > 0$, the mechanical interactions are represented as a delta function at $r = 0$, representing only the formation of open water by divergent ice flow. In pure convergence, $E = (\nabla \cdot u, 0)$ and $\nabla \cdot u < 0$, and mechanical interactions create open water through collisions and $\mathcal{L}_M(r) = |\nabla \cdot u| L_c(r)$. When the ice flow is characterized by shear motions, $\|E\| = \epsilon_{II}$, and collisions still occur due to the differential motion of neighboring floes, which forms open water at a rate of $D_M c/Dt = \epsilon_{II}/2$ per second. Other choices of $D_M c/Dt$ could satisfy Eq. (10), but the Thorndike parameterization meets the intuitive requirements that in pure divergence no collisions occur, while in pure convergence they do, and in pure shear collisions occur such that the rate of open water formation per unit strain is reduced relative to the case of pure convergence.

The effects of mechanical interactions on the FSD are represented by Zhang et al. (2015) similarly to (10), with the rate of area loss (our $D_M c/Dt$) taken from Hibler (1980), and assuming that all floes of different sizes have same ITD. In our joint FSTD formulation, the mechanical interactions are represented for floes characterized by both specific thickness and specific size.

The rearrangement of floe area in response to a unit amount of open water formation, $L_c(r)$, is represented using a collision kernel $K(r_1, r_2; r)$. Let $K(r_1, r_2; r) \, dr_1 \, dr_2 \, dr$ be

A prognostic model of the sea ice floe size and thickness distribution

C. Horvat and
E. Tziperman

Title Page

Abstract	Introduction
Conclusions	References
Tables	Figures

|◄ | ►|

◄ | ►

Back | Close

Full Screen / Esc

Printer-friendly Version

Interactive Discussion

equal to the number of collisions per unit time between floes in the range $(r_1, r_1 + dr_1)$ and floes in the range $(r_2, r_2 + dr_2)$, that form floes in the range $(r, r + dr)$, per unit area of open water formation. In general, the floe number distribution subject to mechanical combination of floes evolves according to

$$\frac{\partial N(r)}{\partial t} = \int\int_{r_1 r_2}\left[\frac{1}{2}N(r_1)N(r_2)K(r_1, r_2; r)\right.$$

$$\left. - N(r)N(r_2)K(r, r_2; r_1)\right] dr_1 dr_2, \tag{15}$$

where the integrals are over all resolved floe sizes. The factor of $1/2$ prevents double-counting: since K is symmetric with respect to its first two arguments, each interaction pair (r_1, r_2) is counted twice in the integral in Eq. (15). This represents the rate of change in the number of floes of size r_3 due to mechanical interactions. The first term on the right-hand side of Eq. (15) represents the increase in floe number at size r due to collisions between floes of other sizes, and the second term represents the loss in floe number at size r due to combination of floes of size r with other floes. Equation (15) is a generalization of the Smoluchowski coagulation equation that has been previously used to model the sea-ice thickness distribution (Godlovitch, 2011). If we multiply Eq. (15) by the area of a floe of size r, we obtain the rate of change of the fractional area covered by floes of size r due to mechanical interactions, which is nothing but the definition of $\mathcal{L}_M(r)$,

$$(\pi r^2)\frac{\partial N(r)}{\partial t} = \mathcal{L}_M(r); \ (r \neq 0). \tag{16}$$

We already concluded above that away from $r = 0$ we have $\mathcal{L}_M(r) = L_c(r)$. Therefore the above equation gives,

$$L_c(r) = (\pi r^2)\frac{\partial N(r)}{\partial t}, \tag{17}$$

where $\partial N/\partial t$ is taken from Eq. (15). We represent the kernel $K(r_1, r_2, r)$ as the product of two factors. The first is the probability of collision via ridging or rafting of two floes of size r_1 and r_2, termed $P_{coll}(r_1, r_2)$ where the subscript "coll" is either "ridge" or "raft", and the probabilities are to be defined more specifically shortly. The second factor is a delta function, $\delta(r - R(r_1, r_2))$, that limits the pairs of collision partners to only those that form a floe of size $r = R(r_1, r_2)$, specified below, and whose area is smaller than the area of the two colliding floes combined. Noting again that the number distribution and area distribution are related through $N(r) = \pi r^2 f(r)$, we combine Eqs. (17) and (15) to find,

$$
L_c(r) = L_c^* \iint_{r_1, r_2} \left[\frac{1}{2} \frac{r^2}{\pi r_1^2 r_2^2} f(r_1) f(r_2) P_{coll}(r_1, r_2) \delta(r - R(r_1, r_2)) \right.
$$

$$
\left. - \frac{1}{\pi r_2^2} f(r) f(r_2) P_{coll}(r, r_2) \delta(r_1 - R(r, r_2)) \right] dr_1 dr_2. \tag{18}
$$

The coefficient L_c^* is a normalization constant ensuring that the integral over $L_c(r)$ is one (Eq. 11). In the discretized version of Eq. (18), two floe classes of discrete size r_1^d and r_2^d which combine to form floes of discrete size r^d do not necessarily satisfy $\pi (r_1^d)^2 h_1^d + \pi (r_2^d)^2 h_2^d = \pi (r^d)^2 h^d$. Ice volume conservation that is independent of the discretization is achieved by determining the newly formed area of the new floes, in each time step, using the constraint that volume must be conserved,

$$
\Delta f \left(r_1^d \right) h_1^d + \Delta f \left(r_2^d \right) h_2^d = -\Delta f \left(r^d \right) h^d,
$$

where $\Delta f(r)$ is the area change at size r in a single timestep due to the mechanical interaction considered here. Thus the total volume lost by floes at size r_1^d and r_2^d (lhs) is equal to the corresponding volume gained at size r_3^d (rhs).

2.2.1 Probability of collision

We choose the functions $P_{coll}(r_1, r_2)$ to be proportional to the probability that two floes of size r_1 and r_2 will overlap if placed randomly in the domain, and they are calculated in a similar manner for both mechanical processes (rafting or ridging). We consider such an overlap as an indication that mechanical interaction has occurred. The area of each floe that may be deformed due to mechanical interactions is restricted to a small region near the edge of the floe, represented in our model by a narrow annulus of width $\delta = \delta_{ridge}$ or $\delta = \delta_{raft}$ at the floe edge, which depends on the floe size and the interaction type. We term these annuli the "contact zones" of the floes, with the interiors being the "cores" (Fig. 1). The area of a single floe of size s is therefore broken down as,

$$\pi s^2 = A_{core}(s) + A_{cz}(s) = \pi(s - \delta)^2 + \pi(2\delta s - \delta^2).$$

The above defined probability of collision between floes of size r_1 and r_2 is proportional to the product of contact zone areas divided by the open ocean area, A, not including the core areas,

$$P_{coll}(r_1, r_2) \propto \frac{A_{cz}(r_1) A_{cz}(r_2)}{(A - A_{core}(r_1) - A_{core}(r_2))^2}.$$

Data of the morphology and width distribution of ridges and rafts as a function of the size of the combining ice floes are scarce, though there are indications that rafts can be substantially larger than ridges (Hopkins et al., 1999). We crudely define the width of the contact zone in ridging to be 5 m, or the size of the smaller of the two combining floes, whichever is smaller,

$$\delta_{ridge}(r_1, r_2) = \min(5\,\text{m}, r_1, r_2).$$

For rafting, we assume a larger portion of the smaller floe may be uplifted, up to 10 m,

$$\delta_{raft}(r_1, r_2) = \min(10\,\text{m}, r_1, r_2).$$

Both choices lead to larger ridges and rafts as the size of the interacting floes increases. Given observations of these processes one can refine the above choices, to which our model is not overly sensitive. Finally, we assume that ridging occurs for floes thicker than 0.3 m, and rafting occurs when both floes are thinner than 0.3 m, consistent with the study of Parmerter (1975), with a smooth transition between the two regimes implemented by a coefficient $\gamma(h)$ which tends to one for thicknesses that are prone to rafting and to zero for ridging,

$$K(r_1, r_2; r) = \gamma(h_1)\gamma(h_2)P_{\text{raft}}(r_1, r_2)\delta(r - R_{\text{raft}}(r_1, r_2))$$
$$+ (1 - \gamma(h_1)\gamma(h_2))P_{\text{ridge}}(r_1, r_2)\delta(r - R_{\text{ridge}}(r_1, r_2)),$$

$$\gamma(h) = \frac{1}{2} - \frac{1}{2}\tanh\left[(h - 0.3)/0.05\right].$$

2.2.2 New floe size

The ice area lost in an interaction is different for rafting and ridging. In rafting, the entire contact zone is replaced by ice whose thickness is the sum of that of the original floes. In ridging, the contact zone is increased in thickness by a factor of 5, compressing its area by a factor of $1/5$ (Parmerter and Coon, 1972). Given that our model assumes each floe has a uniform thickness, we treat floes formed by ridging or rafting to be of uniform thickness, chosen to conserve volume. This choice eliminates the need for keeping track of sea-ice morpology, and as these features occur at the interior of new floes, they are of lesser importance to further mechanical interactions the we assume to occur at floe boundaries. Assuming without loss of generality that $r_1 \leq r_2$, the area of the newly formed floes is therefore given by the sum of the areas minus the area lost to either ridging or rafting. We then divide this area by π and take the square root to find the size of the newly formed floes. The thickness of the formed floe is calculated from

volume conservation. We therefore have,

$$[r, h] = R([r_1, h_1], [r_2, h_2])_{\text{raft}}$$
$$= \left(\sqrt{r_1^2 + r_2^2 - \frac{1}{2} A_{cz,\text{raft}}(r_1)/\pi}, \frac{V(\mathbf{r_1}) + V(\mathbf{r_2})}{\pi r^2} \right),$$

$$[r, h] = R([r_1, h_1], [r_2, h_2])_{\text{ridge}}$$
$$= \left(\sqrt{r_1^2 + r_2^2 - \frac{4}{5} A_{cz,\text{ridge}}(r_1)/\pi}, \frac{V(\mathbf{r_1}) + V(\mathbf{r_2})}{\pi r^2} \right),$$

where $V(\mathbf{r}) = V([r, h]) = h\pi r^2$ is the volume of an ice floe.

2.3 Swell fracture

Sea surface height variations due to surface ocean waves strain and possibly break sea-ice floes into smaller floes of varying sizes. Since this process does not create or destroy sea-ice area, wave-breaking obeys the conservation law,

$$\iint_r \mathcal{L}_W(\mathbf{r}) \, d\mathbf{r} = 0,$$

where $\mathcal{L}_W(\mathbf{r})$ is the time rate of change of floes of size and thickness $\mathbf{r} = (r, h)$ due to wave fracture in Eq. (2), and the integral is over all sizes and thicknesses (a list of the variables used to describe the response of the FSTD to wave fracture is provided in Table 4). Suppose that an area of floes $\Omega(\mathbf{r}, t) \, d\mathbf{r}$ with sizes between $\mathbf{r}$ and $\mathbf{r} + d\mathbf{r}$ is fractured per unit time. Let new floes resulting from this process have the floe size distribution $F(\mathbf{r}, \mathbf{s}) \, d\mathbf{s}$, equal to the fraction of $\Omega(\mathbf{r}, t)$ that becomes floes with size between $\mathbf{s}$ and $\mathbf{s} + d\mathbf{s}$. The rate of change of area of floes of size $\mathbf{r}$ due to wave-breaking

C. Horvat and
E. Tziperman

is then,

$$\mathcal{L}_W(\boldsymbol{r}) = -\Omega(\boldsymbol{r},t) + \int_s \Omega(\boldsymbol{s},t)F(\boldsymbol{s},\boldsymbol{r})\,d\boldsymbol{s}. \tag{19}$$

The first term is the loss of fractional area of size $\boldsymbol{r}$ that is fractured per unit time, and the second is the increase in the area occupied by floes of size $\boldsymbol{r}$ due to the fracture of floes of larger sizes.

Kohout and Meylan (2008) modeled floes as floating elastic plates, and showed ocean surface waves to be attenuated exponentially as a function of the number, Λ, of ice floes the waves encounter as they propagate into an ice pack. Wave energy therefore decays as $\exp(-\alpha\Lambda)$, where the attenuation coefficient is $\alpha(T,\bar{h})$, T is the wave period, and $\bar{h}$ the mean ice thickness. We approximate the number of floes per unit distance as $c(2\bar{r})^{-1}$, where c is the ice concentration and $\bar{r}$ the average effective radius. The attenuation distance, W, is then given by the inverse of the attenuation per floe times the number of floes per unit distance $W(T,\bar{h}) = 2\bar{r}(c\alpha)^{-1}$. We approximate this attenuation by fitting the attenuation coefficient $\alpha(T,\bar{h})$ calculated by Kohout and Meylan (2008) (their Fig. 6) to a quadratic function of the period and mean thickness (Fig. 2). Kohout and Meylan (2008) only report an attenuation coefficient for wave periods longer than 6 seconds and thicknesses less than 3 m (red box in Fig. 2), so we extrapolate to shorter periods and higher thicknesses using this fit when necessary. Our formulation of the effects of wave fracture depends on their wavelengths rather than periods, and we use the deep-water surface gravity wave dispersion relation, $\lambda = gT^2/2\pi$ to convert between the two. Let the width of the domain to which the FSTD model is applied be D (e.g., the width of a GCM grid cell which borders on open water). The fraction of the grid cell area in which waves of wavelength λ may break floes is therefore estimated as $\min(W(\lambda,\bar{h})/D,1)$. The duration $\tau(\lambda)$ over which breaking occurs is approximated as the domain width divided by the group velocity for surface gravity

waves,

$$\tau(\lambda) = \frac{D}{c_g(\lambda)} = 2D\sqrt{\frac{2\pi}{g\lambda}}.$$

We assume floes flex with the sea surface height, and for a monochromatic and unidirectional wave field of wavelength λ and amplitude a, the maximal strain of a floe of thickness h occurs at the crest and trough of the wave, with magnitude $\epsilon_{max} = a\,h2\pi^2/\lambda^2$ (Dumont et al., 2011, p. 4). If the maximum strain exceeds an empirically defined value ϵ_{crit}, the floe will break, and since the maximum strain occurs between the trough and crest of the wave, the fracture leads to floes of size $\lambda/2$. If the wavelength is larger than the floe radius, the floe will not be fractured.

The amplitude of waves with wavelengths in the range λ to $\lambda + d\lambda$ is approximated as $a(\lambda) \approx \sqrt{S(\lambda)\,d\lambda}$, where $S(\lambda)$ is the normalized wave energy spectrum (in units of m, see WMO, 1998, p. 11). The spectrum $S(\lambda)d\lambda$ represents the total wave energy belonging to waves with wavelengths between λ and $\lambda + d\lambda$, normalized by ρg.

Since many wavelengths can fracture a floe of a given effective radius r, information about the likelihood distribution of wave heights $P_{\text{wa}}(a)da$, the probability of a wave amplitude lying in the range a to $a + da$, is used to complete the formulation. Observations of wave amplitudes (see Michel, 1968, p. 19) show wave heights to be Rayleigh distributed,

$$P_{\text{wa}}(a) = \frac{2a}{H_s^2}\exp\left(-a^2/H_s^2\right).$$

The probability $P_f(\mathbf{r},\lambda)$ that a floe of size $\mathbf{r}$ fractures due to a wave of wavelength λ is therefore chosen as,

$$P_f(\mathbf{r},\lambda) = \begin{cases} A^{-1}P_{\text{wa}}(a(\lambda)) & \text{if } \epsilon_{\text{crit}} > \epsilon_{max}(\lambda,\mathbf{r}) \text{ and } \lambda < r, \\ 0 & \text{otherwise.} \end{cases} \tag{20}$$

The normalization by $A(\mathbf{r}) = \int P_{\mathrm{wa}}(a(\lambda))\theta(\epsilon_{\mathrm{crit}}(\lambda, \mathbf{r}) - \epsilon_{\mathrm{max}})\theta(r - \lambda)\mathrm{d}\lambda$, where $\theta(x)$ is the Heaviside step function, assures that the integral of P_{f} over all wavelengths is equal to 1 if the floes of size $\mathbf{r}$ will break. Since the wavelength required to form a floe of size r is $\lambda = 2r$, the size distribution of floes resulting from the fracture of floes of size $\mathbf{s}$, $F(\mathbf{s}, \mathbf{r})$, is equal to

$$F(\mathbf{s}, \mathbf{r}) = F\left((s, h_{\mathrm{s}}), (r, h_r)\right) = P_{\mathrm{f}}((s, h_{\mathrm{s}}), 2r)\delta(h_{\mathrm{s}} - h_r),$$

where the first term is the probability that a floe of size (s, h_{s}) will be fractured by a wave of wavelength $\lambda = 2r$, and the delta function represents the fact that ice that is fractured does not change its thickness. The function $\Omega(\mathbf{r}, t)\mathrm{d}\mathbf{r}$, which is the fractional area fractured per unit time that belongs to floes of size between r and $r + \mathrm{d}r$, can now be written,

$$\Omega(\mathbf{r}, t) = \int \frac{1}{\tau(\lambda)} \min\left(\frac{W(\lambda, \overline{h})}{D}, 1\right) P_{\mathrm{f}}(\mathbf{r}, \lambda)\,\mathrm{d}\lambda.$$

The first two factors under the integral sign represent the rate at which waves enter the domain, and the fractional area of the domain that they reach. This is multiplied by the probability that such waves are observed and will fracture floes of size $\mathbf{r}$, which depends on the wave spectrum in the marginal ice zone. Waves that attenuate rapidly are less capable of breaking a large area of floes.

   The effects of wave fracture on the FSD is represented by Zhang et al. (2015) based on an expression similar to Eq. (19), assuming that only floes with horizontal size larger than a specified threshold break, that a fractured floe is equally likely to form any smaller size within a specified range, and that all floes in a given size class have the same ITD. In the representation in the present paper of the effects of wave fracture on the joint FSTD, the wave spectrum plays a central role in determining the resulting floe sizes, as well as the propagation distance over which ocean waves are attenuated by the ice field. Information about the specific thickness of individual floe sizes informs the strain rate failure criterion and therefore determines which floes will be fractured.

3 Model results

To demonstrate and understand the model's response to a variety of forcing scenarios, we first examine its response over a single time step in three runs with idealized forcing fields. Each of these scenarios applies one of the following forcing fields: a net surface cooling $Q = -100\,\mathrm{W\,m^{-2}}$ which induces ice growth, a rate of ice flow convergence of $\nabla \cdot \boldsymbol{u} = -5 \times 10^{-9}\,\mathrm{s^{-1}}$ which induces floe collisions, and a surface gravity wave field of a single wavelength $\lambda = 56\,\mathrm{m}$ and amplitude of $1\,\mathrm{m}$, leading to wave fracture. The model is initialized with a size and thickness distribution composed of two Gaussian peaks (Fig. 3a). The first (referred to as size I below) has a mean size of $90\,\mathrm{m}$ and a mean thickness of $0.25\,\mathrm{m}$. Ice at this size and thickness is susceptible to swell fracture and rafting. The second peak (size II) has a mean size of $15\,\mathrm{m}$ and a mean thickness $1.5\,\mathrm{m}$. Ice at this size and thickness tends to ridge rather than raft, and is not susceptible to wave fracture given our specified wave field. This second point is important, as it demonstrates a possible scenario in which knowledge of the ITD and FSD, seperately, would not be sufficient to evolve the FSTD, as some floes, independent of their thickness, will not fracture. The initial sea-ice concentration is 75 %. The domain width is $D = 10\,\mathrm{km}$, and the width of the lead region is set to be $r_{\mathrm{p}} = 0.5\,\mathrm{m}$, the smallest floe size resolved in this model. The critical strain amplitude for flexural failure, e_{crit}, is set to 3×10^{-5} in line with other studies (Kohout and Meylan, 2008; Dumont et al., 2011).

When two floes of size r and s combine due to rafting or riding interactions, they form a new floe with effective radius $r' > \max(r, s)$. For an arbitrary floe size discretization into size bins, this new size may not lie within a bin representing a size larger than those of the two interacting floes. As a result, interacting floes may accumulate at a single bin size rather than move into bins representing larger sizes. The minimum bin resolution necessary to avoid this problem is set by the interaction of two floes that are the same size r, with r smaller than the ridge width δ_{ridge}. When two such small floes interact via ridging in our model, one of them becomes 5 times thicker and

its area is reduced by a factor of 5. They therefore form a floe of size $\sqrt{6/5}r$. We select a variable discretization, with $r_{n+1} = \sqrt{6/5}r_n$, with 26 floe sizes between 0.5 and 156 m. There are 14 thickness categories, 13 of which are equally spaced between 0.1 to 2.5 m. To conserve volume when thick floes combine or grow due to freezing, the 14th thickness category incorporates all thicknesses greater than 2.5 m.

The difference between the model state after a single one-hour time step and the model initial conditions is shown in Fig. 3b–d. Cooling leads to growth in both thickness and size (Fig. 3b) with the impact of lateral growth being less visible than the change in thickness. The shift in thickness is seen by the negative tendency (blue shading) for thicknesses smaller than the maximum of the initial distribution, and positive tendency at sizes larger than the initial maximum (red shading). These tendencies correspond to the shifting of floes from thinner to thicker floes due to the freezing. The shift in horizontal size is less apparent in the figure, due to the separation of scales between size and thickness: lateral growth rates are comparable to vertical growth rates ($1\,\mathrm{cm\,day^{-1}}$), but given that there is more than an order of magnitude difference between the floe size and thickness, the size change corresponds to a smaller relative change than the thicknesses change. The size response would be more apparent for smaller initial floe sizes not included in this idealized model experiment.

Mechanical interactions (Fig. 3c) lead to growth at three distinct clusters of size and thickness. The first, due to the self-interaction (rafting) of floes of size I, is shown as a positive tendency at a floe size of 123 m and thickness of 0.35 m. The second cluster is due to a ridging interaction between floes of size I and II, leading to new floes of around 90 m size and 0.5 m thickness. The third, due to self-interaction (ridging) between floes of size II, leads to a positive tendency at floe sizes around 17 m and thickness around 1.7 m.

Swell fracture (Fig. 3d) leads to the fracturing of many of the floes of size I, shown as a negative tendency at the eliminated size class. Floes of size II are not affected because they are smaller than twice the wavelength of the specified surface gravity

wave field. Since the specified wave field is monochromatic, the area of floes of size I that are broken is shown as a positive tendency at a floe size equal to half of the wavelength of the surface gravity wave, $\lambda/2 = 28$ m. Ice thickness does not change during wave fracture.

Next, two one-month simulations are performed using the same initial distribution to show the behavior of the model forced by two different fixed strain rate scenarios (Fig. 4). The first (Fig. 4a and b) simulates convergence of fixed magnitude ($\epsilon_\text{I} = -10^{-7}, \epsilon_\text{II} = 0$) s^{-1}, and the second (Fig. 4c and d) simulates shear of fixed magnitude ($\epsilon_\text{I} = 0, \epsilon_\text{II} = 10^{-7}$) s^{-1}. When there is no convergence, the rate of open water formation due to collisions (Eq. 13) is 0.5×10^{-7} s^{-1}, equal to the magnitude of the strain rate tensor divided by two,

$$\left.\frac{D_\text{M}c}{Dt}\right|_\text{shear} = \frac{1}{2}\left(\epsilon_\text{I} - \|E\|\right) = -\frac{1}{2}\|E\|.$$

When there is no shear, and only convergence, the amount of open water formation due to collisions is 10^{-7} s^{-1}, equal to the magnitude of the strain rate tensor,

$$\left.\frac{D_\text{M}c}{Dt}\right|_\text{conv} = \frac{1}{2}\left(\epsilon_\text{I} - \|E\|\right) = -\frac{1}{2}\left(|\epsilon_\text{I}| + |\epsilon_\text{I}|\right) = -\|E\|.$$

In both scenarios the norm of the strain rate tensor is the same, $\|E\| = 10^{-7}$ s^{-1}. In the case of only shear (Fig. 4c and d), ice concentration is diminished by a factor of roughly 18 %, corresponding to a 22 % increase in mean ice thickness, and with no change in ice volume. In contrast, in the case of convergence only (Fig. 4a and b), ice concentration is diminished by 36 %, with a corresponding 56 % increase in mean ice thickness, again with no change in ice volume. Thus shear motions lead to collisions and the combinations of floes with one another, but at a reduced rate when compared to convergence of ice flow, for the same strain rate tensor norm. In the case of shear only, the two initial peaks in the FSTD are smeared out over a range of floe sizes

and thicknesses (Fig. 4b), with the variety of floe sizes and thicknesses increasing in number over time. Since there is twice as much open water formation in the case of convergence only, and therefore an increased number of mechanical interactions, the distribution of floe sizes and thickness is smeared more rapidly, and over a larger range (Fig. 4c).

Figure 5 shows the response of the joint floe size and thickness distribution to a single-week experiment that simulates a seven-day period of wave fracture, using a wave spectrum that leads to ice breaking into a broader range of floe sizes. The experiment uses the Bretschneider (Michel, 1968, p. 24) surface wave spectrum as function of period T, $S(T)\,\mathrm{d}T$,

$$
S(T)\,\mathrm{d}T = \frac{1 H_s^2}{4\pi T_z}\left(\frac{T}{T_z}\right)^3 e^{-\frac{1}{\pi}\left(\frac{T}{T_z}\right)^4}\,\mathrm{d}T,
$$

where $H_s = 2\,\mathrm{m}$ is the significant wave height (the mean wave height of the 1/3 highest surface waves), and $T_z = 6\,\mathrm{s}$ is the mean time interval between zero-crossings of the observed wave record. We use the surface gravity wave dispersion relation $\lambda = gT^2/2\pi$ to write $S(T)\,\mathrm{d}T$ as a wavelength spectrum $S(\lambda)\,\mathrm{d}\lambda$. The wavelength bins are spaced to correspond uniquely to floe size bins, and there is a one-to-one relationship between a wave's wavelength and the floe size of new floes formed through fracture of existing floes by that wave. The peak wavelength of the wave spectrum is at $T \approx 7.5\,\mathrm{s}$, corresponding to $\lambda \approx 88\,\mathrm{m}$. As before, the domain width D is set to $10\,\mathrm{km}$. Large floes (size I) are rapidly fractured, with the fractional area corresponding to these floes is decreasing, and the distribution shifts towards smaller sizes (Fig. 5a, gray lines). After one week, the fractional area belonging to floes in the range from 75–125 m decreases from 37 to less than 1 %, with mean floe size decreasing by 58 % (Fig. 5b, blue line). As a consequence, the total lateral surface area rises as floes are broken and their lateral sides are exposed, increasing by 47 % over the week (Fig. 5b, blue line). Over time continual fracture eliminates large floes and replaces them with smaller floes, leading

Title Page

Abstract | Introduction

Conclusions | References

Tables | Figures

◄ | ►

◄ | ►

Back | Close

Full Screen / Esc

Printer-friendly Version

Interactive Discussion

to an increase in lateral surface area by 220 % and a decrease in mean floe size of 73 %.

4   Conclusions

The sea-ice floe size and thickness distribution (FSTD) may play an important role in the context of climate studies, influencing air–sea exchange, oceanic and atmospheric circulation, and sea-ice dynamics, area and thickness evolution. As ice thins, feedbacks that take place on scales smaller than the typical climate model grid scale, between the lateral sizes of floes, thermodynamic melting and freezing along floe sides and bases, ocean waves and floe collisions, may affect climate on larger scales. In addition to the FSTD being an interesting and under-explored dynamical problem, it is therefore also important to study it, develop appropriate parameterizations and represent it in global climate models.

We developed a model that simulates the evolution of the FSTD, using as input large-scale oceanic and atmospheric forcing fields, which may be useful as an extension to sea-ice models presently used in global climate models. We included representations of the impact of thermodynamics (melting and freezing), mechanical interactions of rafting and ridging due to floe collisions, and of floe fracture by ocean surface waves, all processes that are active in marginal or seasonal sea-ice zones. We demonstrated the effect of these processes using model runs forced by external forcing fields including air–sea heat flux, ice flows leading to mechanical interactions, and specified surface wave field, and considered the effects of these forcing fields individually and when combined. We demonstrated the effects of mechanical interactions in the presence of both shearing and straining ice flows, separately accounting for ridging and rafting. We studied the effect of surface waves, first for idealized single-wavelength wave fields, and then accounting for a more realistic surface wave spectrum. We examined the response to melting and freezing both along existing floe bases and lateral edges, and in open water, leading to pancake ice formation.

While the present paper focuses on the development of parameterizations needed to represent the FSTD dynamics and to testing the model with individual forcing fields, we hope to next study the consequences of realistic forcing fields on the FSTD and compare model output to the few available observations. Another important future direction is the model development and testing that will allow for implementation of this model into sea-ice models used in GCMs, allowing for realistic ice thermodynamics, constitutive stress-strain relationship, wave model, and ice motions driven by ocean currents and winds. At the same time, an implementation into a GCM would require making the model more efficient by replacing the high resolution we could afford to use here in floe size and thickness by a simplified approach, possibly assuming a functional form of the FSTD and simulating only its moments as is often done in atmospheric models of the particle size distribution.

The study of FSTD dynamics, and the development of a prognostic FSTD model, are made difficult by the scarcity of observations of the floe size distribution and its seasonal and long term evolution. Such observations are required to constrain uncertain parameters used in the model developed here, and help determine the dominant processes which need to be included in FSTD models to be incorporated in global climate models.

Appendix: Comparison of rate constants in Eq. 14 to those in Thorndike et al. (1975)

Thorndike et al. (1975) employed the following parameterization of the function ψ (Eq. 1), which represents the rate of change of area belonging to ice of thickness h due to mechanical interactions:

$$\psi = \left(\epsilon_\mathrm{I}^2 + \epsilon_\mathrm{II}^2 \right)^{1/2} \left(\alpha_0 \delta(h) + \alpha_r w_r(h) \right), \tag{1}$$

where $\int_0^\infty w_r(h) = -1$, and the coefficients α_0 and α_c are,

$$\alpha_0 = \frac{1}{2}\left(1 + \cos(\theta)\right), \tag{2}$$

$$\alpha_c = \frac{1}{2}\left(1 - \cos(\theta)\right), \tag{3}$$

where $\theta = \arctan(\epsilon_{\mathrm{II}}/\epsilon_{\mathrm{I}})$. Using the trigonometric identity,

$$\cos(\arctan(\epsilon_{\mathrm{II}}/\epsilon_{\mathrm{I}})) = \frac{\epsilon_{\mathrm{I}}}{\|E\|},$$

with $\|E\| \equiv \sqrt{\epsilon_{\mathrm{I}}^2 + \epsilon_{\mathrm{II}}^2}$, ψ may be rewritten as,

$$\psi = \frac{1}{2}\|E\|\left(\delta(h)\frac{\|E\| + \epsilon_{\mathrm{I}}}{\|E\|} + \frac{\|E\| - \epsilon_{\mathrm{I}}}{\|E\|}w_r\right), \tag{4}$$

$$= \frac{1}{2}\left(\delta(h)(\|E\| + \epsilon_{\mathrm{I}}) + w_r(\|E\| - \epsilon_{\mathrm{I}})\right), \tag{5}$$

$$= \delta(h)\epsilon_{\mathrm{I}} + \frac{1}{2}\left(\|E\| - \epsilon_{\mathrm{I}}\right)\left(\delta(h) + w_r\right). \tag{6}$$

Identifying $w_r = -\int_h L_c(r)\,\mathrm{d}h$, and $\frac{1}{2}\left(\|E\| - \epsilon_{\mathrm{I}}\right) = \frac{D_{\mathrm{M}}c}{Dt}$, recovers the floe-size-integrated form of Eq. (14).

References

Asplin, M. G., Galley, R., Barber, D. G., and Prinsenberg, S.: Fracture of summer peren-
   nial sea ice by ocean swell as a result of Arctic storms, J. Geophys. Res., 117, 1–12,
   doi:10.1029/2011JC007221, 2012. 2957

5 Asplin, M. G., Scharien, R., Else, B., Howell, S., Barber, D. G., Papakyriakou, T., and Prinsen-
   berg, S.: Implications of fractured Arctic perennial ice cover on thermodynamic and dynamic
   sea ice processes, J. Geophys. Res. Oceans, 119, 2327–2343, doi:10.1002/2013JC009557,
   2014. 2957

Birnbaum, G. and Lüpkes, C.: A new parameterization of surface drag in the marginal sea ice
10   zone, Tellus A, 54, 107–123, doi:10.1034/j.1600-0870.2002.00243.x, 2002. 2958

Bitz, C. M.: Numerical modeling of sea ice in the climate system, Tech. Rep., University of Wash-
   ington, availagle at: www.atmos.uw.edu/~bitz/Bitz_chapter.pdf (last access: 22 May 2015),
   2008. 2958

Bitz, C. M., Holland, M. M., Weaver, A. J., and Eby, M.: Simulating the ice-thickness distribution
15   in a coupled climate model, J. Geophys. Res., 106, 2441, doi:10.1029/1999JC000113, 2001.
   2958

Bourke, R. H. and Garrett, R. P.: Sea ice thickness distribution in the Arctic Ocean, Cold Reg.
   Sci. Technol., 13, 259–280, doi:10.1016/0165-232X(87)90007-3, 1987. 2958

Cavalieri, D. J. and Parkinson, C. L.: Arctic sea ice variability and trends, 1979–2010, The
20   Cryosphere, 6, 881–889, doi:10.5194/tc-6-881-2012, 2012. 2956

Chevallier, M. and Salas-Mélia, D.: The role of sea ice thickness distribution in the arctic sea
   ice potential predictability: a diagnostic approach with a coupled GCM, J. Climate, 25, 3025–
   3038, doi:10.1175/JCLI-D-11-00209.1, 2012. 2958

Collins, C. O., Rogers, W. E., Marchenko, A., and Babanin, A. V.: In situ measurements of an
25   energetic wave event in the Arctic marginal ice zone, Geophys. Res. Lett., 42, 1863–1870,
   doi:10.1002/2015GL063063, 2015. 2957

Dumont, D., Kohout, A., and Bertino, L.: A wave-based model for the marginal ice
   zone including a floe breaking parameterization, J. Geophys. Res., 116, C04001,
   doi:10.1029/2010JC006682, 2011. 2959, 2975, 2977

30 Feltham, D. L.: Granular flow in the marginal ice zone, Philos. T. R. Soc. A, 363, 1677–1700,
   doi:10.1098/rsta.2005.1601, 2005. 2957

Godlovitch, D., Illner, R., and Monahan, A.: Smoluchowski coagulation models of sea ice thickness distribution dynamics, J. Geophys. Res., 116, 2156–2202, doi:10.1029/2011JC007125, 2011. 2969

Girard, L., Weiss, J., Molines, J. M., Barnier, B., and Bouillon, S.: Evaluation of high-resolution sea ice models on the basis of statistical and scaling properties of Arctic sea ice drift and deformation, J. Geophys. Res., 114, C08015, doi:10.1029/2008JC005182, 2009. 2958

Harvey, L. D. D.: Testing alternative parameterizations of lateral melting and upward basal heat flux in a thermodynamic sea ice model, J. Geophys. Res., 95, 7359–7365, doi:10.1029/JC095iC05p07359, 1990. 2964

Henderson, G. R., Barrett, B. S., and Lafleur, D.: Arctic sea ice and the Madden–Julian Oscillation (MJO), Clim. Dynam., 43, 2185–2196, doi:10.1007/s00382-013-2043-y, 2014. 2956

Herman, A.: Sea-ice floe-size distribution in the context of spontaneous scaling emergence in stochastic systems, Phys. Rev. E., 81, 066123, doi:10.1103/PhysRevE.81.066123, 2010. 2959

Hibler, W. D.: A dynamic thermodynamic sea ice model, J. Phys. Oceanogr., 9, 815–846, doi:10.1175/1520-0485(1979)009<0815:ADTSIM>2.0.CO;2, 1979. 2958

Hibler III, W. D.: Modeling a variable thickness ice cover, Mon. Weath. Rev., 108, 1943–1973, 1980. 2968

Holt, B. and Martin, S.: The effect of a storm on the 1992 summer sea ice cover of the Beaufort, Chukchi, and East Siberian Seas, J. Geophys. Res., 106, 1017–1032, doi:10.1029/1999JC000110, 2001. 2959

Hopkins, M. A., Tuhkuri, J., and Lensu, M.: Rafting and ridging of thin ice sheets, J. Geophys. Res., 104, 13605–13613, doi:10.1029/1999JC900031, 1999. 2971

Horvat, C. and Tziperman, E.: Effects of the sea ice floe size distribution on Polar ocean properties and air–sea exchange, 2014 Fall Meeting, AGU, San Francisco, Calif., 15–19 December 2014, C11A-0341, 2014. 2957

Hunke, E. C., Lipscomb, W. H., Turner, A. K., Jeffery, N., and Elliot, S.: CICE: The Los Alamos Sea Ice Model Documentation and SoftwareUsers Manual Version 5.0, Tech. rep., Los Alamos Natl. Laboratory, Los Alamos, N.M., 2013. 2958

Johannessen, J. A., Johannessen, O. M., Svendsen, E., Shuchman, R., Manley, T., Campbell, W. J., Josberger, E. G., Sandven, S., Gascard, J. C., Olaussen, T., Davidson, K., and Van Leer, J.: Mesoscale eddies in the Fram Strait marginal ice zone during

the 1983 and 1984 Marginal Ice Zone Experiments, J. Geophys. Res., 92, 6752–6772, doi:10.1029/JC092iC07p06754, 1987. 2957

Kohout, A. L. and Meylan, M. H.: An elastic plate model for wave attenuation and ice floe breaking in the marginal ice zone, J. Geophys. Res., 113, C09016, doi:10.1029/2007JC004434, 2008. 2974, 2977, 2994

Lu, P., Li, Z. J., Zhang, Z. H., and Dong, X. L.: Aerial observations of floe size distribution in the marginal ice zone of summer Prydz Bay, J. Geophys. Res., 113, C02011, doi:10.1029/2006JC003965, 2008. 2959

McPhee, M. G.: Turbulent heat flux in the upper ocean under sea ice, J. Geophys. Res., 97, 5365–5379, doi:10.1029/92JC00239, 1992. 2964

Michel, W. H.: Sea Spectra Simplified, Marine Technol., 5, 17–30, 1968. 2975, 2980, 2997

Niebauer, H.: Wind and melt driven circulation in a marginal sea ice edge frontal system: a numerical model, Cont. Shelf Res., 1, 49–98, doi:10.1016/0278-4343(82)90032-2, 1982. 2957

Parkinson, C. L. and Washington, W. M.: A large-scale numerical model of sea ice, J. Geophys. Res., 84, 311–337, doi:10.1029/JC084iC01p00311, 1979. 2964

Parmerter, R. R.: A model of simple rafting in sea ice, J. Geophys. Res., 80, 1948–1952, doi:10.1029/JC080i015p01948, 1975. 2972

Parmerter, R. R. and Coon, M. D.: Model of pressure ridge formation in sea ice, J. Geophys. Res., 77, 6565–6575, doi:10.1029/JC077i033p06565, 1972. 2972

Perovich, D. K. and Jones, K. F.: The seasonal evolution of sea ice floe size distribution, J. Geophys. Res. Oceans, 119, 8767–8777, doi:10.1002/2014JC010136, 2014. 2959

Renner, A. and Gerland, S.: Evidence of Arctic sea ice thinning from direct observations, Geophys. Res. Lett., 2012, 5029–5036, doi:10.1002/2014GL060369.1, 2014. 2958

Rothrock, D. A. and Thorndike, A. S.: Measuring the sea ice floe size distribution, J. Geophys. Res., 89, 6477–6486, doi:10.1029/JC089iC04p06477, 1984.

Semtner, A. J.: A Model for the thermodynamic growth of sea ice in numerical investigations of climate, J. Phys. Oceanogr., 6, 379–389, doi:10.1175/1520-0485(1976)006<0379:AMFTTG>2.0.CO;2, 1976. 2958

Steele, M.: Sea ice melting and floe geometry in a simple ice-ocean model, J. Geophys. Res., 97, 17729–17738, doi:10.1029/92JC01755, 1992. 2957, 2964

Steer, A., Worby, A., and Heil, P.: Observed changes in sea-ice floe size distribution during early summer in the western Weddell Sea, Deep-Sea Res. II, 55, 933–942, doi:10.1016/j.dsr2.2007.12.016, 2008. 2959

A prognostic model of the sea ice floe size and thickness distribution

C. Horvat and
E. Tziperman

Title Page

Abstract	Introduction
Conclusions	References
Tables	Figures

|◄ | ►|

◄ | ►

Back | Close

Full Screen / Esc

Printer-friendly Version

Interactive Discussion

Stroeve, J. C., Serreze, M. C., Holland, M. M., Kay, J. E., Malanik, J., and Barrett, A. P.: The Arctic's rapidly shrinking sea ice cover: a research synthesis, Climatic Change, 110, 1005–1027, doi:10.1007/s10584-011-0101-1, 2012. 2957

Strong, C. and Rigor, I. G.: Arctic marginal ice zone trending wider in summer and narrower in winter, Geophys. Res. Lett., 40, 4864–4868, doi:10.1002/grl.50928, 2013. 2957

Strong, C., Magnusdottir, G., and Stern, H.: Observed feedback between winter sea ice and the North Atlantic Oscillation, J. Climate, 22, 6021–6032, doi:10.1175/2009JCLI3100.1, 2009. 2956

Thorndike, A. S., Rothrock, D. A., Maykut, G. A., and Colony, R.: The thickness distribution of sea ice, J. Geophys. Res., 80, 4501–4513, doi:10.1029/JC080i033p04501, 1975. 2958, 2967, 2968, 2982

Toyota, T. and Enomoto, H.: Analysis of sea ice floes in the Sea of Okhotsk using ADEOS/AVNIR images, in: Proceedings of the 16th IAHR International Symposium on Ice, International Association of Hydraulic Engineering and Research, 211–217, 12 February 2012–12 June 2012, Dunedin, New Zealand, 2002. 2959

Toyota, T., Takatsuji, S., and Nakayama, M.: Characteristics of sea ice floe size distribution in the seasonal ice zone, Geophys. Res. Lett., 33, L02616, doi:10.1029/2005GL024556, 2006. 2959

Toyota, T., Haas, C., and Tamura, T.: Size distribution and shape properties of relatively small sea-ice floes in the Antarctic marginal ice zone in late winter, Deep-Sea Res. II, 58, 1182–1193, doi:10.1016/j.dsr2.2010.10.034, 2011. 2959

Vavrus, S. J., Holland, M. M., Jahn, A., Bailey, D. A., and Blazey, B. A.: Twenty-first-century arctic climate change in CCSM4, J. Climate, 25, 2696–2710, doi:10.1175/JCLI-D-11-00220.1, 2012. 2957

Washington, W. M., Semtner, A. J., Parkinson, C., and Morrison, L.: On the development of a seasonal change sea-ice model, J. Phys. Oceanogr., 5, 679–685, doi:10.1175/1520-0485(1976)006<0679:OTDOAS>2.0.CO;2, 1976. 2964

Williams, T. D., Bennetts, L. G., Squire, V. A., Dumont, D., and Bertino, L.: Wave–ice interactions in the marginal ice zone, Part 1: Theoretical foundations, Ocean Model., 71, 81–91, doi:10.1016/j.ocemod.2013.05.010, 2013. 2959

WMO: Guide to Wave Analysis and Forecasting, World Meteorological Organization, Geneva, Switzerland, 1998. 2975

Title Page

Abstract | Introduction

Conclusions | References

Tables | Figures

◀ | ▶

◀ | ▶

Back | Close

Full Screen / Esc

Printer-friendly Version

Interactive Discussion

Wu, Q. and Zhang, X.: Observed evidence of an impact of the Antarctic sea ice dipole on the Antarctic oscillation, J. Climate, 24, 4508–4518, doi:10.1175/2011JCLI3965.1, 2011. 2956

Yu, Y. and Rothrock, D. A.: Thin ice thickness from satellite thermal imagery, J. Geophys. Res., 101, 25753–25766, doi:10.1029/96JC02242, 1996. 2958

Zhang, J., Lindsay, R., Schweiger, A., and Steele, M.: The impact of an intense summer cyclone on 2012 Arctic sea ice retreat, Geophys. Res. Lett., 40, 720–726, doi:10.1002/grl.50190, 2013. 2957

Zhang, J., Schweiger, A., Steele, M., and Stern, H.: Sea ice floe size distribution in the marginal ice zone: theory and numerical experiments, J. Geophys. Res. Oceans, doi:10.1002/2015JC010770, in press, 2015. 2959, 2962, 2968, 2976

Table 1. Variables appearing in several components of the FSTD model.

Variable	Description	Section
$g(h)$	Ice thickness distribution (ITD)	1
$\boldsymbol{u}$	Ice velocity vector	1
ψ	Ice thickness redistribution function	1
$n(r)$	Ice floe size distribution (FSD)	1
$\boldsymbol{r} = (r, h)$	Floe size and thickness	1
$f(\boldsymbol{r})$	Joint floe size and thickness distribution (FSTD)	1
ϕ	Open water fraction	2.1
c	Ice concentration	2.1
$N(\boldsymbol{r})$	Floe number distribution	2.1
$C(\boldsymbol{r})$	Cumulative floe number distribution	2.1

Table 2. Variables used in the representation of thermodynamical processes in the FSTD model.

Variable	Description	Section
$\mathcal{L}_\mathrm{T}$	Thermodynamic component of FSTD model	1
G	Ice size and thickness growth rate	2.1
$(r_\mathrm{p}, h_\mathrm{p})$	Size of smallest ice pancakes	2.1
A_lead	Lead area fraction	2.1
Q_lead	Lead area heat flux	2.1
Q_o	Open water heat flux	2.1
$\dot{A}_\mathrm{p}$	Rate of pancake area growth	2.1
$Q_\mathrm{l,l}$	Fraction of lead heat flux transmitted to floe sides	2.1
$Q_\mathrm{l,b}$	Fraction of lead heat flux transmitted to floe bases	2.1

Table 3. Variables used in the representation of mechanical interactions in the FSTD model.

Variable	Description	Section
$\mathcal{L}_M$	Mechanical component of FSTD model	1
D_M/Dt	Rate of change incorporating ice collisions	2.2
L_c	Normalized fraction of concentration lost/gained by collisions	2.2
$\dot{e}$	Ice flow strain rate tensor	2.2
E	Vector of strain rate tensor invariants	2.2
$K(r_1, r_2, r)$	Collision kernel: two floes of size r_1 and r_2 forming a floe of size r	2.2
$P_{coll}(r_1, r_2)$	Probability of two floes of sizes r_1 and r_2 colliding	2.2
$\delta_{raft/ridge}$	Width of contact zone for collisions rafting/ridging	2.2
A_{cz}	Area of floe contact zone	2.2
A_{core}	Area of floe core	2.2
$\gamma(h)$	Interpolation coefficient between rafting and ridging	2.2

Table 4. Variables used in the representation of wave fracture in the FSTD model.

Variable	Description	Section
$\mathcal{L}_M$	Wave fracture component of FSTD model	1
$\Omega(r,t)$	Area of floes of size r fractured by waves	2.3
$F(r,s)$	Floe size and thickness distribution of new floes formed by the wave fracture of floes of size r	2.3
$\alpha(\lambda,h)$	Attenuation coefficient (per floe) for waves of wavelength λ encountering ice of thickness h	2.3
D	Width of computational domain onto which waves are incident	2.3
$\tau(\lambda)$	Timescale for waves of wavelength λ to cross domain	2.3
$P_f(r,\lambda)$	Probability that floes of size r will break due to waves of wavelength λ	2.3
$S(\lambda)$	Incident wave spectrum	2.3
$a(\lambda)$	Amplitude of waves of wavelength λ	2.3
ϵ_{crit}	Critical strain rate for breaking of floes	2.3
$\epsilon_{max}(\lambda,h)$	Maximal strain rate experienced by a floe of thickness h due to waves of amplitude $a(\lambda)$	2.3
H_s	Significant wave height (height of 1/3 highest waves)	2.3
P_{wa}	Rayleigh distribution of surface wave heights	2.3
T_z	Zero-crossing period for wave record	3
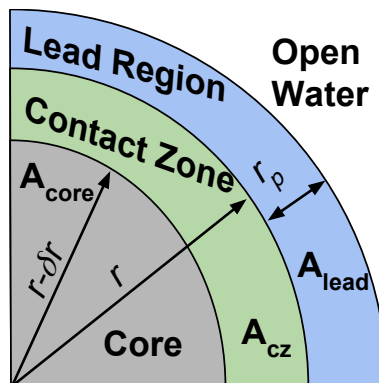
Figure 1. A section of a floe, showing the division of a floe and the surrounding sea surface for the thermodynamic and mechanical interaction components of the FSTD model. The floe itself, of radius r, is divided into the core which is unaffected by ridging and rafting (blue, width $r - \delta r$) and contact zone which participates in these interactions (green, width δr). The floe is surrounded by the lead region of width r_p where net heat fluxes lead to freezing or melting of the floe itself (blue) and then by open water where cooling may lead to new pancake ice formation (white).

C. Horvat and E. Tziperman
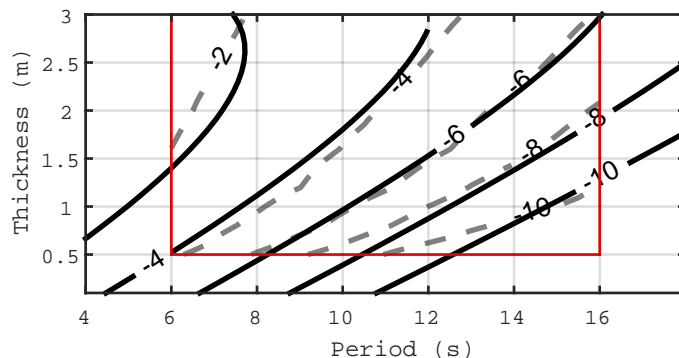
Figure 2. The natural logarithm of the attenuation coefficient α calculated by Kohout and Meylan (2008) (dash, inside the red box) and a quadratic fit to this attenuation coefficient that is used in Sect. 2.3 (solid). Solid contours outside of the red box are extrapolated using the quadratic fit. The fit is given by $\ln\alpha(T,\bar{h}) = -0.3203 + 2.058\bar{h} - 0.9375T - 0.4269\bar{h}^2 + 0.1566\bar{h}T + 0.0006T^2$.
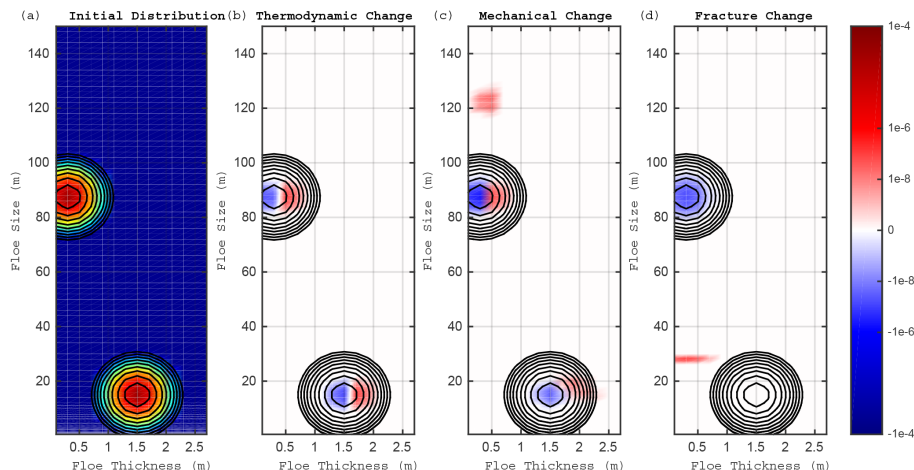
Figure 3. Response of the FSTD to idealized single-process experiments over a single time step (Sect. 3). **(a)** Change in response to thermodynamic forcing only. **(b)** Change in response to mechanical forcing only. **(c)** Change in response to wave fracture forcing only. Solid black contours in **(a–c)** show the initial floe size and thickness distribution, and contour intervals are powers of ten. Right color bar corresponds to the change in the FSTD in units of fractional area per timestep ($1\,\mathrm{s}^{-1}$). Warm colors indicate an increase in fractional area, cool colors indicate a decrease in fractional area.
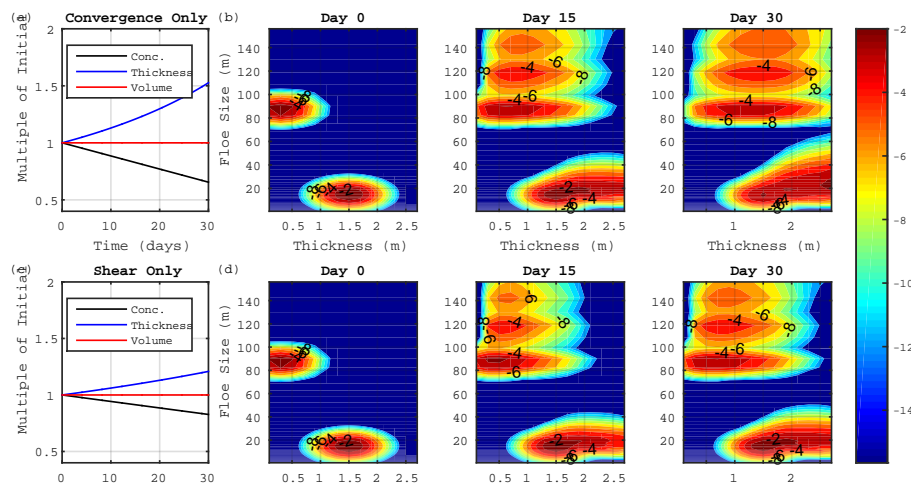
Figure 4. Results of two simulations of the floe size and thickness distribution forced with fixed ice-flow strain rates and only mechanical interactions. **(a)** Ice concentration, mean thickness, and ice volume for one month of fixed shear, with no convergence. Timeseries are normalized by their initial values. **(b)** The base 10 logarithm of the FSTD at days 0, 15, and 30 for the run with only shear. Color bar corresponds to base 10 logarithm of the FSTD, contour intervals are powers of ten. **(c and d)** Same as **(a and b)** for one week of fixed convergence with no shear.
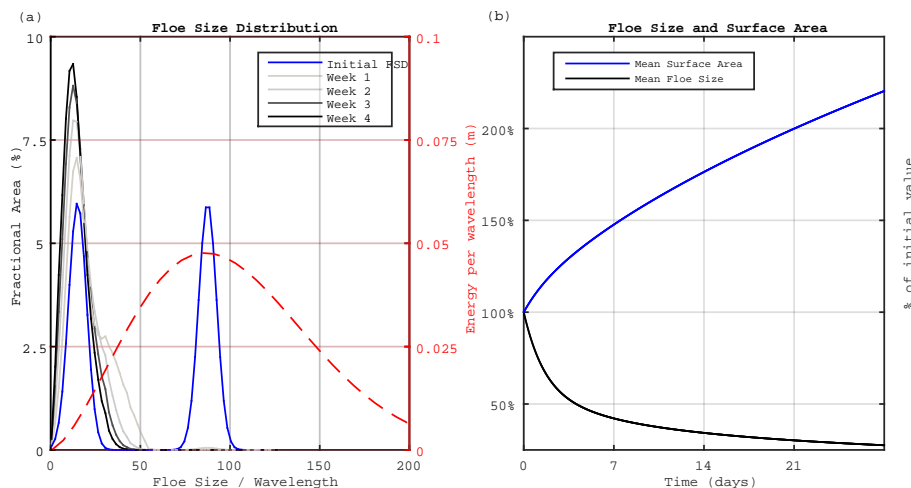
Figure 5. Results of simulations of the FSTD forced with swell fracture only. **(a)** The FSD before (black line, left axis) and after (grey lines line, left axis) each week of swell fracture using a Bretschneider (Michel, 1968, p. 23) wave spectrum (dashed red line, right axis). As swell fracture does not affect floe thickness, the distribution is plotted as a function of floe size only. **(b)** The mean floe size and total lateral ice surface area as a fraction of their initial values over the course of one week of wave fracture with the specified wave spectrum.